

# Nanoworm BiVO<sub>4</sub> Photoelectrochemical Sensor Prepared by a Cyanuric-Chloride-Assisted Sol-Gel Process and Its Sensing Property for Ascorbic Acid

Yi-Ye Liu, Yong-Hao Xiao, and Wei-De Zhang\*

School of Chemistry and Chemical Engineering, South China University of Technology, 381 Wushan Road, Guangzhou, 510640, People's Republic of China

\*E-mail: [zhangwd@scut.edu.cn](mailto:zhangwd@scut.edu.cn)

Received: 15 June 2018/ Accepted: 20 August 2018 / Published: 5 January 2019

---

A nanoworm BiVO<sub>4</sub> photoanode was successfully synthesized by sol-gel drop-casting for the determination of ascorbic acid. The structure and surface morphology of the obtained samples were characterized, and their photoelectrochemical properties and sensing performance towards ascorbic acid were investigated. The precursor solids were also investigated, and the results proved that cyanuric chloride, which was bound with other precursors, generated the nanoworm morphology. The nanoworm BiVO<sub>4</sub> photoanode enhanced the photocurrent density and exhibited a sensitivity of 68.9  $\mu\text{A mM}^{-1} \text{cm}^{-2}$  towards ascorbic acid with high selectivity under visible light illumination.

---

**Keywords:** BiVO<sub>4</sub> photoanode, Nanoworm, Sol-gel method, Cyanuric chloride, Photoelectrochemical sensor, Ascorbic acid.

## 1. INTRODUCTION

Ascorbic acid (AA), which is found in various foods and is known to be a powerful antioxidant, protects human organs and other tissues by scavenging excess free radicals. The determination of AA plays a vital role in detecting human diseases and developing correspondingly effective medicines [1, 2]. Over several decades, novel electrochemical sensors for AA determination with excellent sensitivities and broad linear ranges have been developed. However, most electrochemical sensors have exhibited low sensitivities towards AA in the low concentration region (<300  $\mu\text{M}$ ). Photoelectrochemical (PEC) analysis has the characteristics of a low background signal and high sensitivity towards antioxidants, owing to its separation of the excitation source and detection signal, and is a promising method for AA determination [3-8].

With its suitable semiconductor bandgap of 2.4-2.6 eV for absorbing abundant visible light from solar illumination, bismuth vanadate (BiVO<sub>4</sub>) is a potential choice serving as the electrode in

electrochemical sensors. Moreover, BiVO<sub>4</sub> has many advantages including easy synthesis, low cost, environmental compatibility, and high stability [9-11]. Therefore, it has been widely applied in gas sensing, water splitting, organic pollutant degradation and CO<sub>2</sub> reduction [12-15]. Recently, BiVO<sub>4</sub> PEC sensors for H<sub>2</sub>O<sub>2</sub> and antioxidative substances including AA have been reported [16, 17]. However, it is essential to design and fabricate nanostructured BiVO<sub>4</sub> sensors to further improve both the photocurrent and sensitivity for the potential application of these sensors in wearable electronics [18]. According to previous reports, nanoporous BiVO<sub>4</sub> photoanodes with worm-like morphology exhibited a remarkable PEC performance [19, 20]. The multiple light diffractions and larger surface areas of nanoporous structures accounted for the enhancement of the light harvesting [21]. To date, two strategies for the synthesis of nanoworm BiVO<sub>4</sub> photoanodes have been reported. The first is to convert BiOI electrodes to BiVO<sub>4</sub> photoanodes with worm-like structures due to the sufficient voids between the BiOI thin plates; however, this approach is complicated and time-consuming [20, 22]. The second strategy is to use sol-gel drop-casting with the introduction of a morphology-directing agent into the precursor solutions; in contrast to the first strategy, this approach is facile and inexpensive [21]. While it was reported that polyethylene glycol 600 (PEG600) and polyethyleneimine (PEI) can be used as the morphology-directing agents [22, 23], syntheses of nanoworm BiVO<sub>4</sub> photoanodes involving small molecules have rarely been attempted. Moreover, BiVO<sub>4</sub> composite electrodes with metal oxide semiconductors such as TiO<sub>2</sub>/BiVO<sub>4</sub>, WO<sub>3</sub>/BiVO<sub>4</sub> and ZnO/BiVO<sub>4</sub> on metal oxide substrates exhibited excellent PEC performance [24-26]. To enhance charge transfer in the electrodes, a binder is desirable to connect the precursors of BiVO<sub>4</sub> with the substrates or other metal oxide semiconductors during the preparation process.

Cyanuric chloride (C<sub>3</sub>N<sub>3</sub>Cl<sub>3</sub>, denoted as CC) is an important and inexpensive chloride reagent in organic syntheses due to the reactivity of its chloride atoms towards nucleophiles. Thus, CC can react with a variety of hydroxyl and carboxylic compounds including polyethylene glycol [27, 28]. Furthermore, metal oxides including SnO<sub>2</sub> and TiO<sub>2</sub> can chemically adsorb CC due to the surface hydroxyls [29, 30]. Thus, CC is a good choice for use as a binder to interconnect the organics and metal oxide of the precursors in the synthesis of nanoworm BiVO<sub>4</sub> electrodes using morphology-directing agents.

In this study, a nanoworm BiVO<sub>4</sub> photoelectrochemical sensor for AA detection was fabricated via low-cost and facile sol-gel chemistry coupled with drop-casting. The binder CC was introduced into the precursor solution. Thermal treatment with the precursor solution was conducted to generate precursor networks [31, 32]. The performance characteristics of the prepared PEC sensors were studied, and the influence of CC on the precursor networks, surface morphology, PEC properties and sensitivity to AA was investigated and discussed in detail.

## 2. EXPERIMENTAL

### 2.1 Reagents

In this study, FTO-coated glasses (14 W cm<sup>-2</sup>) with the area of 1×3 cm<sup>2</sup> were purchased from Nippon Sheet, Japan. The glasses were ultrasonicated successively in acetone, ethanol and deionized

water and were rinsed with ethanol prior to use.  $\text{Bi}(\text{NO}_3)_3 \cdot 5\text{H}_2\text{O}$  was obtained from Tianjin Kemiou Chemical Reagent Co., Ltd. (Tianjin, China). Vanadyl acetylacetonate ( $\text{VO}(\text{acac})_2$ ) and cyanuric chloride (CC) were purchased from Aladdin. Ethylene glycol was purchased from Chinasun Specialty Products Co., Ltd. (China). Phosphate buffer solution (PBS, 0.10 M, pH=6.5) was prepared by fully mixing 0.10 M  $\text{Na}_2\text{HPO}_4$  (126 mL), 0.10 M  $\text{NaH}_2\text{PO}_4$  (274 mL) and NaCl (3.60 g).  $\text{Na}_2\text{HPO}_4$ ,  $\text{NaH}_2\text{PO}_4$ ,  $\text{Na}_2\text{SO}_4$  and NaCl were purchased from Guangdong Guanghua Chemical Factory Co., Ltd. (Guangzhou, China). Ascorbic acid was purchased from Tianjin Kemiou Chemical Reagent Co., Ltd. (Tianjin, China). Deionized (DI) water (resistivity  $>18.4 \text{ M}\Omega \text{ cm}^{-1}$ ) was prepared using a GWA-UN 1-10 water purifier.

## 2.2 Materials synthesis

The photoanode denoted as BVO-CC was prepared by sol-gel drop-casting procedure reported in previous work with modifications[21]. First, bismuth nitrate pentahydrate ( $\text{Bi}(\text{NO}_3)_3 \cdot 5\text{H}_2\text{O}$ , 1.2 mmol) was dissolved in ethylene glycol (16 mL) under stirring to obtain solution "A". Then, vanadyl acetylacetonate ( $\text{VO}(\text{acac})_2$ , 1.2 mmol) and cyanuric chloride (CC, 3.6 mmol) were dissolved into ethylene glycol ( $(\text{CH}_2\text{OH})_2$ , EG, 24 mL) by sonication to obtain solution "B". The precursor solution with 30 mM  $\text{Bi}^{3+}$  was formed by fully mixing solution "A" with solution "B". The precursor solution was transferred into an 80 mL Teflon-lined autoclave and maintained at 160 °C for 12 h and then cooled down to room temperature naturally. The resultant lawn green solution without any solid was stored in a dark and cool environment. The precursor solution (180  $\mu\text{L}$ ) was drop-cast on an FTO substrate followed by drying at 160 °C for 40 min and then cooling. Then, the sample was washed several times with ethanol and water. Finally, the sample was dried at 80 °C and successively calcined at 500 °C for 2.5 h in a muffle furnace with a ramp rate of 2 °C  $\text{min}^{-1}$ . The photoanode denoted as BVO was prepared following a similar procedure except that no CC was introduced into the precursor solution.

To further study the effect of CC, the precursor particles were synthesized by directly drying the precursor solution. In this process, the resultant mixture (10 mL) was transferred into a porcelain boat and evaporated at 180 °C for 8 h in an oven. The resultant particles were washed several times with ethanol and water and dried at 80 °C. The products corresponding to the precursor solutions of BVO and BVO-CC were denoted as BVO-p and BVO-CC-p, respectively.

## 2.3 Characterization

Scanning electron microscopy (SEM) images of the samples were obtained using a scanning electron microscope (SEM, Merlin, Zeiss). The X-ray powder diffraction (XRD) patterns were obtained using a Bruker GADDS diffractometer (Cu  $K\alpha$  radiation) in the  $2\theta$  range from 10 to 70°. UV-vis diffuse reflectance spectroscopy (UV-vis DRS) measurements were conducted using a Hitachi U3010 spectrophotometer with  $\text{BaSO}_4$  as the baseline. Fourier transform infrared (FTIR) spectra were recorded using an IR Affinity-1 FTIR spectrometer at the frequencies from 4000 to 400  $\text{cm}^{-1}$  and KBr pellets were used as the matrix. The PEC measurements of the electrodes were carried out in a conventional three-electrode cell using a CHI660C electrochemical workstation (Chenhua, Shanghai). In the three-electrode

system, the BiVO<sub>4</sub>/FTO electrode (with an exposed surface area of 1.0 cm × 0.8 cm to the electrolyte), Ag/AgCl electrode and Pt foil served as the working electrode, the reference electrode and the counter electrode, respectively. A 300 W Xenon lamp (PLS-SXE 300/300UV, Beijing Perfectlight Technology Co. Ltd, China) with a 420 nm cut-off filter provided visible light illumination with an intensity of 100 mW cm<sup>-2</sup>. Electrochemical impedance spectroscopy (EIS) was conducted under the applied potential. The frequency range was between 10000 and 0.01 Hz, the applied amplitude was 10 mV, and the redox probe was K<sub>3</sub>[Fe(CN)<sub>6</sub>]/K<sub>4</sub>[Fe(CN)<sub>6</sub>] (2.5/2.5 mM). The measured Nyquist plots were fitted with an equivalent circuit using the ZSim software.

#### 2.4 PEC determination of AA

All of the experiments for AA determination were conducted with an amperometric method based on the PEC measurements. In each of the experiments, AA solution (10 μL) with a concentration of 0.02, 0.04 or 0.1 M was successively injected into the PBS (20 mL) electrolyte, accounting for the AA additions with concentrations of 10, 20 or 50 μM, separately. The current data were collected at 40 s after the previous additions. The current densities were calculated with the equation:  $j = i/A$ , where  $i$  is the current,  $j$  is the current density, and  $A$  is the working area (0.8 cm<sup>2</sup>) of the electrodes.

### 3. RESULTS AND DISCUSSION

The surface morphologies of BVO-CC and BVO were observed by SEM. BVO displayed a porous structure with narrow slits (Fig. 1a).

As shown in Fig. 2b, a characteristic worm-like network composed of nanoworm particles with the width of ca. 100 nm was obtained. The SEM images reveal that adding CC into the precursor solution resulted in a nanoworm structure.

To identify the crystal phases of BVO-CC and BVO, XRD measurements were conducted (Fig. 3c). The diffraction peaks at  $2\theta$  of 26.4° and 37.7° are attributed to stannic oxide (SnO<sub>2</sub>, JCPDS card No. 77-0450), while the peaks at 18.8°, 28.7° and 30.8° are indexed to monoclinic bismuth vanadate (BiVO<sub>4</sub>, JCPDS card No. 14-0688). All of the characteristic diffraction peaks were found in the patterns of both BVO-CC and BVO [21], demonstrating that both BVO-CC and BVO were monoclinic BiVO<sub>4</sub> photoanodes. Moreover, the ratio of the intensities of the (040) crystal lattice peak and the (121) crystal lattice peak of monoclinic BiVO<sub>4</sub> was greater in the pattern of BVO-CC than in that of BVO. This observation revealed that BVO-CC grew with a preferred orientation along the (040) crystal plane[33].

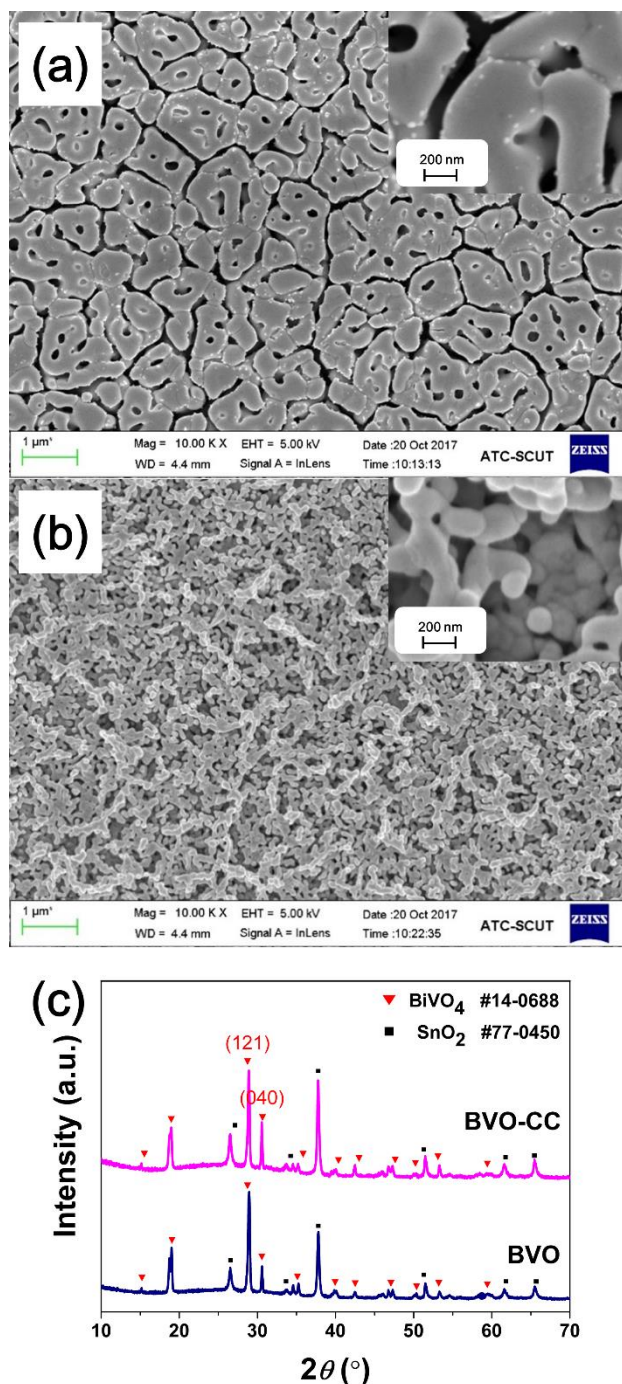


**Figure 4.** SEM images of (a) BVO and (b) BVO-CC with insets showing high-resolution images. (c) XRD patterns of BVO and BVO-CC.

The precursor networks were explored by XRD and FTIR on BVO-p and BVO-CC-p to reveal the formation mechanism of the nanoworm structure. The XRD pattern of BVO-p indicated an amorphous structure (Fig. 5a). Only low intensity diffraction peaks were observed at  $2\theta$  of  $27.8^\circ$  and  $28.7^\circ$ , which were indexed to tetragonal  $\text{Bi}_2\text{O}_3$  (JCPDS no. 27-0050) and monoclinic  $\text{BiVO}_4$  (JCPDS no. 14-0688). In the BVO-CC-p pattern, diffraction peaks at  $2\theta$  of  $19.6^\circ$  and  $29.7^\circ$  had strong intensity. Both peaks were assigned to  $\text{Bi}_4\text{V}_6\text{O}_{21}$  (JCPDS no. 33-0222).

Fig. 6b shows the FT-IR spectra of BVO-p and BVO-CC-p. The broad band at 3300-3700  $\text{cm}^{-1}$  of BVO-p and BVO-CC-p was assigned to the O-H stretching vibrations. The weak band at 1580-1680  $\text{cm}^{-1}$  of BVO-p was indexed to the C-O bond of the residual  $\text{VO}(\text{acac})_2$ . The strong peaks corresponding to V=O (1405  $\text{cm}^{-1}$ ), V-O (773  $\text{cm}^{-1}$ ) and Bi-O (530  $\text{cm}^{-1}$ ) bonds of BVO-CC were found in the spectrum of BVO-CC, in agreement with the XRD results [34, 35]. The band at 3100-3250  $\text{cm}^{-1}$ , the peak at 1457  $\text{cm}^{-1}$  and the peak at 810  $\text{cm}^{-1}$  were attributed to the N-H stretching,  $\text{sp}^2 \text{C}=\text{N}-\text{C}$  bonds and triazine rings, respectively. These characteristic responses confirm the presence of triazine rings of CC in BVO-CC [32, 36, 37]. In contrast to BVO, the peak at 2990  $\text{cm}^{-1}$  that was assigned to the  $-\text{CH}_3$  groups, the very strong peaks at 1600-1795  $\text{cm}^{-1}$  corresponding to the C=O bonds and the band at 2750-2900  $\text{cm}^{-1}$  assigned to the  $-\text{CH}_2-$  stretching modes were found in the FTIR spectrum of BVO-CC [38].

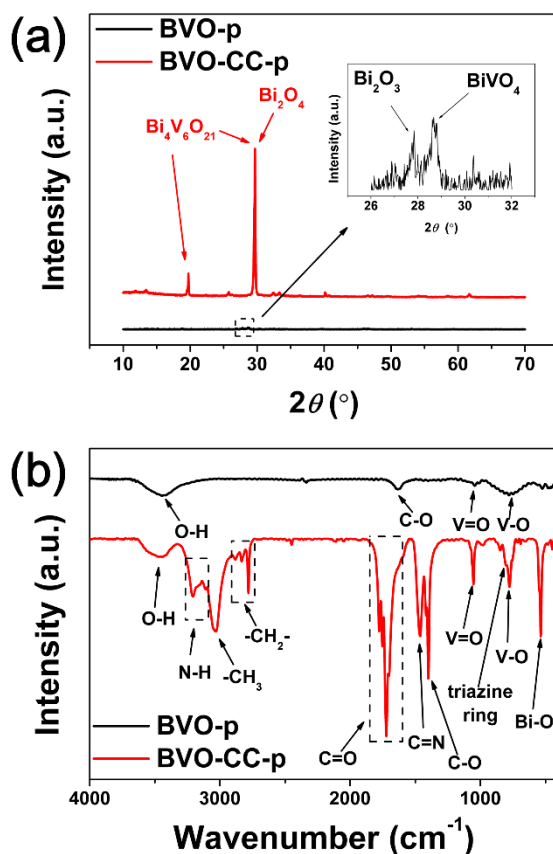


**Figure 7.** (a) XRD patterns of BVO-p and BVO-CC-p. (b) FTIR spectra of BVO-p and BVO-CC-p

It was reported that  $\text{VO}(\text{acac})_2$  was converted to vanadyl ethylene glycolate ( $\text{VO}(\text{OCH}_2\text{CH}_2\text{O})$ ) in a thermal process using EG as a solvent [39]. EG tended to become coordinated with  $[\text{VO}]^{2+}$  during the thermal process, and acetylacetonate ( $\text{Hacac}$ ) was generated. In addition,  $\text{Bi}^{3+}$  in the EG solution formed a stable bismuth ethylene glycolate ( $\text{Bi}_2(\text{OCH}_2\text{CH}_2\text{O})_3$ ) complex because of its strong coordination with ionized EG. The possible reaction equation is displayed as follows:  $\text{VO}(\text{acac})_2 + \text{HOCH}_2\text{CH}_2\text{OH} \rightarrow \text{VO}(\text{OCH}_2\text{CH}_2\text{OH}) + 2\text{Hacac}$  [40]. The strong peaks in the XRD pattern of BVO-CC implied that the Bi-V-O, Bi-O and V-O compounds exhibited high crystallinity in presence of CC. It was suggested that CC bound the  $[\text{VO}]^{2+}$  and  $\text{Bi}^{3+}$  species that were coordinated with ethylene

glycolate due to the substitution of its reactive chlorine atoms by hydroxyl groups. Therefore, the introduction of CC gave rise to the oriented crystal configuration of Bi-V-O, Bi-O and V-O compounds. Among all of the compounds in the solution, methyl groups ( $-\text{CH}_3$ ) and carbonyl groups ( $\text{C}=\text{O}$ ) were found only in Hacac.

It was inferred from the appearance of the  $-\text{CH}_3$  groups and  $\text{C}=\text{O}$  bonds in the IR spectrum of BVO-CC-p that Hacac or acetylacetonate ( $\text{acac}^-$ ) was linked to the precursor networks with the help of CC.

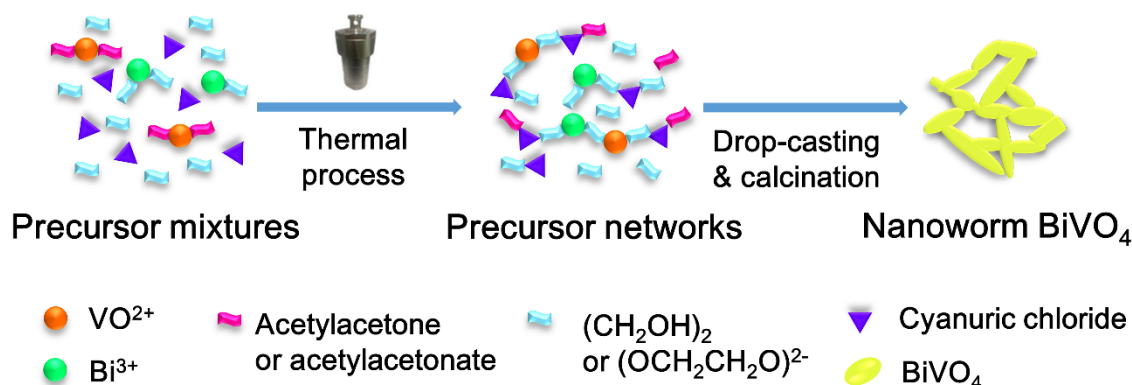


**Figure 8.** Schematic illustration of the synthetic procedure for the nanoworm  $\text{BiVO}_4$  PEC sensor (BVO-CC).

The  $\text{C}=\text{O}$  bonds attached to the precursor compounds connect to the hydroxyl groups in EG *via* hydrogen bonds ( $-\text{C}=\text{O}\cdots\text{H}-\text{O}-$ ), contributing to the total dissolution of the precursor networks in EG[39]. Overall, the introduction of CC into the precursor solution accounted for the construction of the precursor networks consisting of metal ethylene glycolate, CC and Hacac. The decomposition of the precursor networks accounted for the nanoworm morphology of BVO-CC during the calcination process [22]. The possible generation of the  $\text{BiVO}_4$  nanoworm structure is illustrated in Fig. 9.

To reveal the light absorption properties of the photoanodes, the optical characteristics of BVO and BVO-CC were investigated by UV-vis DRS (Fig. 10a). Although the absorption edges of both BVO and BVO-CC were similarly located ca. 502 nm, BVO-CC exhibited higher absorbance than BVO in the 350-550 nm region. The bandgap of a direct transition semiconductor is calculated according to:  $(\alpha h\nu)^2 = A(h\nu - E_g)$ , where  $\alpha$  is the absorption coefficient,  $A$  is a constant,  $\nu$  is the light frequency, and  $E_g$  is the semiconductor bandgap [19, 41]. From the inset plots, the bandgaps of BVO-CC and BVO were calculated as 2.60 and 2.62 eV, respectively. Therefore, a slight optical enhancement of the  $\text{BiVO}_4$  photoanode was obtained after the addition of CC.

Electrochemical impedance spectroscopy (EIS) was carried out to study the charge transfer properties of BVO-CC and BVO. Nyquist plots of the photoanodes in the absence and presence of visible illumination were recorded (Fig. 11b). The Nyquist plot of BVO-CC showed a smaller EIS radius than that of BVO, indicating that the photogenerated charges could easily transfer to the electrolyte. The data can be fitted to an equivalent circuit consisting of a constant phase element (CPE), solution resistance ( $R_s$ ) and charge-transfer resistance ( $R_{ct}$ ) as shown in the inset [42]. The charge-transfer resistance values

for BVO and BVO-CC obtained from the fitting circuits are 2.98 and 2.38 k $\Omega$ , respectively. In other words, BVO-CC showed a lower charge transfer resistance than BVO. It can be concluded from the Nyquist plots that cyanuric chloride in the precursor solution plays a significant role in enhancing the charge transfer efficiency of the BiVO<sub>4</sub> photoanode.

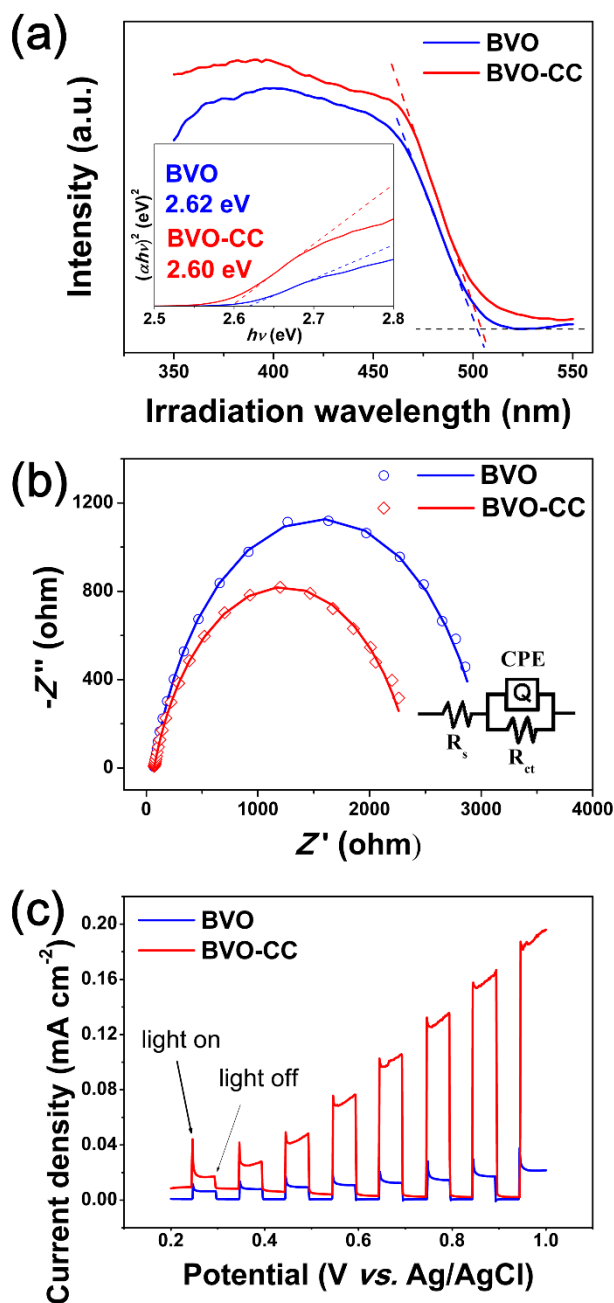


**Figure 12.** (a) UV-Vis DRS spectra of BVO and BVO-CC. Inset: the corresponding  $(\alpha h\nu)^2-h\nu$  plot. (b) EIS plots of BVO and BVO-CC in 0.10 M PBS containing  $\text{K}_3[\text{Fe}(\text{CN})_6]/\text{K}_4[\text{Fe}(\text{CN})_6]$  (2.5/2.5 mM) under visible illumination. Symbol: measured data. Line: fitted data. Inset: the equivalent circuit. (c) Chopped linear sweep voltammograms for BVO and BVO-CC in 0.10 M  $\text{Na}_2\text{SO}_4$  solution under visible light illumination at a scan rate of 10  $\text{mV s}^{-1}$ .

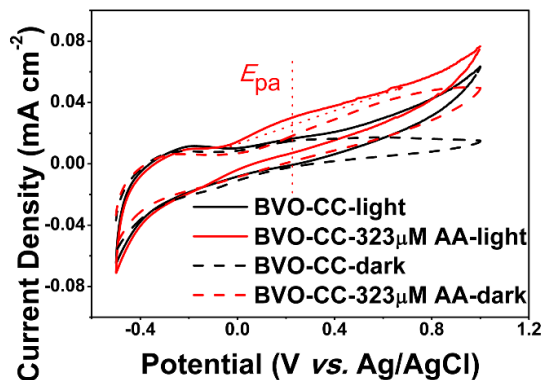


**Figure 13.** Cyclic voltammograms of BVO-CC with and without addition of 323  $\mu\text{M}$  AA in the absence and presence of visible light illumination.  $E_{pa}$ : potential of anodic peak, +0.23 V (vs. Ag/AgCl)

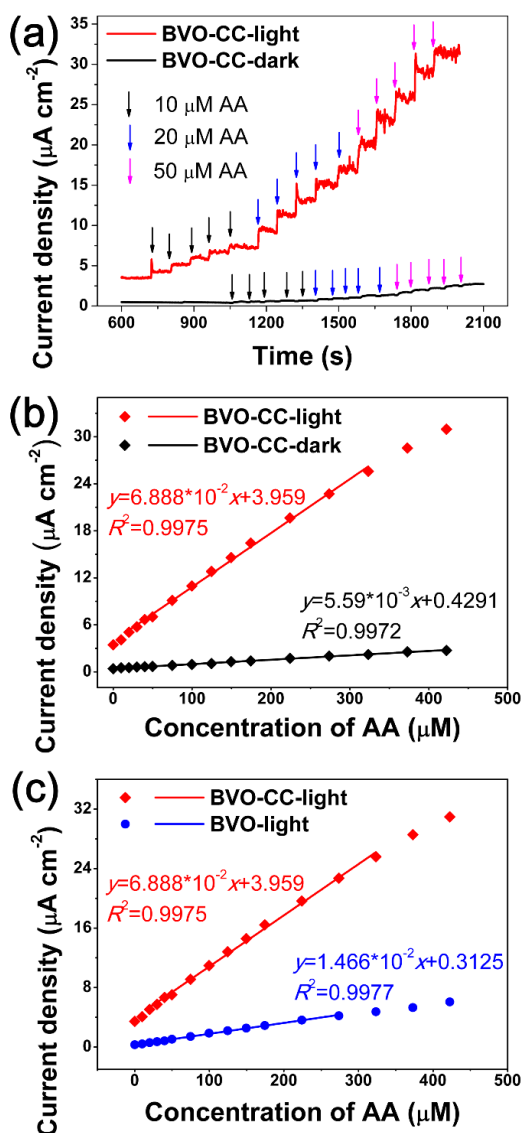


**Figure 14.** (a) Amperometric curves of BVO-CC in 0.10 M PBS at +0.23 V in response to successive additions of AA with and without illumination. (b) Concentration-dependent current responses of BVO-CC with and without illumination. (c) Concentration-dependent photocurrent responses of BVO and BVO-CC.

Photocurrent densities were obtained from chopped linear sweep voltammetry (LSV) in 0.1 M Na<sub>2</sub>SO<sub>4</sub> in the potential range from -0.2 to +0.6 V (vs. Ag/AgCl) at a scan rate of 10 mV s<sup>-1</sup> (Fig. 15c). Apparently, BVO-CC exhibited a higher current density than BVO under visible light illumination. Moreover, the enhancement in the current density of BVO-CC with the increase of the potential was higher than that for BVO.

The effect of AA on the PEC sensor BVO-CC with and without visible light illumination was investigated by cyclic voltammetry (CV) in 0.10 M PBS (pH=6.5) (Fig. 16). Both in the absence and in the presence of illumination, the addition of 323 μM AA into the electrolyte improved the current density of BVO-CC in the voltage range of 0.2-1.0 V (vs. Ag/AgCl). Under visible light illumination, introducing AA enhanced the photocurrent density of BVO-CC in a broader voltage range from -0.05 to 1.0 V. The anodic peak in the cyclic voltammogram of BVO-CC with the addition of 323 μM AA under illumination was found at the potential ( $E_{pa}$ ) of +0.23 V.

**Table 1.** Methods, sensitivities and linear ranges of different electrodes for the determination of AA.

Sensor	Methods	Sensitivity (μA mM <sup>-1</sup> cm <sup>-2</sup> )	Linear range (μM)	R <sup>2</sup>	Ref.
CoPd/C/GCE <sup>a</sup>	Electrochemistry	1179	0.1-3420	0.9926	[2]
GNSs/PPF <sup>b</sup>	Electrochemistry	261.7	400-6000	0.997	[43]
NG/GCE <sup>c</sup>	Electrochemistry	80.90	10-1600	0.9994	[44]
GS/GNR/GCE <sup>d</sup>	Electrochemistry	22.2	10-360	0.9908	[45]
HNP-PtTi alloy/GCE <sup>e</sup>	Electrochemistry	5.48	450-1000	0.9651	[46]
ZnO/Ag/Mn <sub>2</sub> O <sub>3</sub> /GCE <sup>f</sup>	Electrochemistry	114.3	400-700	0.994	[6]
Mo-BiVO <sub>4</sub> /GCE <sup>g</sup>	Photoelectrochemistry	6.096	12.46~327.1	0.987	[16]
Nanoworm BiVO <sub>4</sub> /FTO <sup>h</sup>	Photoelectrochemistry	68.89	19.98-323.3	0.9975	(This work)

a. Cobalt-palladium/carbon modified glassy carbon electrode.

b. Graphene nanosheets on pyrolysed photoresist film.

c. Nitrogen-doped graphene modified glassy carbon electrode.

d. Graphene sheet/graphene nanoribbon modified glassy carbon electrode.

e. Hierarchical nanoporous PtTi alloy modified glassy carbon electrode.

f. ZnO/Ag/Mn<sub>2</sub>O<sub>3</sub> hybrid material modified glassy carbon electrode.

g. Molybdenum-doped BiVO<sub>4</sub> modified glassy carbon electrode.

h. Nanoworm BiVO<sub>4</sub> on fluorine-doped tin oxide glass.

Photoelectrochemical determination of AA was performed using the amperometric method. The current-time curves of BVO-CC at +0.23 V in response to the successive addition of AA with and without illumination are presented in Fig. 17a. Corresponding to the current-time curves, the calibration curves of the current density to AA concentration are displayed in Fig. 18b. Under visible light illumination, BVO-CC exhibited a high sensitivity of 68.89 μA mM<sup>-1</sup> cm<sup>-2</sup> in the linear range of 19.98-323.3 μM (R<sup>2</sup>=0.9975), and the detection limit was 8.74 μM (S/N=3). Compared to the results listed in Table 2, the nanoworm BiVO<sub>4</sub> electrode displayed a better or comparable sensitivity under a low concentration of

300  $\mu\text{M}$ . In the dark, the electrode showed a low sensitivity of  $5.59 \mu\text{A mM}^{-1} \text{cm}^{-2}$  with the linear range of 9.98-447.1  $\mu\text{M}$ . Apparently, visible light illumination is beneficial for the detection of AA by BVO-CC. In addition, the sensitivity of BVO-CC was also compared to that of BVO in order to demonstrate the effect of CC. The calibration curves of the photocurrent responses to the AA concentration are displayed in Fig. 19c. The sensitivity of BVO was  $14.66 \mu\text{A mM}^{-1}$  in the linear range of 9.98-273.7  $\mu\text{M}$ , which was less than that of BVO-CC. The statistical data for AA determination are listed in Table 3. According to the results of our investigation, the presence of CC in the precursor solution improved the sensitivity of the nanoworm  $\text{BiVO}_4$  electrode under illumination for AA determination.

**Table 4.** Current densities of BVO-CC in light, BVO-CC in dark and BVO in light for AA determination

AA Concentration / $\mu\text{M}$	Current density ( $\mu\text{A cm}^{-2}$ ) of BVO-CC-light	Current density ( $\mu\text{A cm}^{-2}$ ) of BVO-CC-dark	Current density ( $\mu\text{A cm}^{-2}$ ) of BVO-light
0	3.453	0.395	0.311
9.995	4.096	0.516	0.413
19.98	5.060	0.532	0.595
29.95	5.744	0.620	0.715
39.92	6.667	0.660	0.836
49.88	7.108	0.692	1.056
74.79	9.117	0.821	1.417
99.70	10.96	0.941	1.860
124.6	12.81	1.062	2.201
149.5	14.58	1.303	2.543
174.3	16.44	1.399	2.904
224.0	19.64	1.729	3.627
273.7	22.71	2.018	4.209
323.3	25.60	2.219	4.751
372.8	28.56	2.548	5.313
422.4	30.96	2.732	6.073

In various biological samples, some interferents such as saccharides and organic acids normally coexist with ascorbic acid (AA) and may hinder the specific determination of AA [2]. To verify the specificity of our sensor, the interference study on BVO-CC was conducted. Under visible light illumination, the current responses were measured with successive addition of 0.1 mM AA each time and 0.2 mM interferents including lactic acid (LA), malic acid (MA), oleic acid (OA), lactose (LT), sucrose (SC) and fructose (FT) (Fig. 20). The results revealed that the current responses towards the examined interferents on BVO-CC sensor can be neglected. Moreover, BVO-CC electrode still exhibits a significant current response towards AA after the addition of the interferents. It is evident that BVO-CC exhibits high selectivity in the determination of AA.

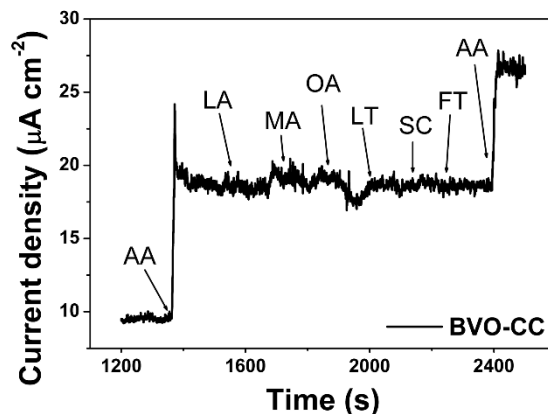


**Figure 21.** Interference tests of BVO-CC in 0.10 M PBS at +0.23 V with AA and other interferents.

The possible working mechanism of the nanoworm  $\text{BiVO}_4$  PEC sensor (BVO) was proposed and is illustrated in Fig. 8. When the  $\text{BiVO}_4$  sensor is exposed to visible light illumination, its nanoworm structure with the large surface area increases the optical absorbance. Photo-generated electron-hole pairs are excited due to the suitable bandgap. Meanwhile, the AA in the electrolyte that captured the excited holes is oxidized to dehydroascorbic acid (DA), while the photocurrent signals are generated from the excited electrons. The nanoworm structure of the  $\text{BiVO}_4$  sensor provides a large surface area for the contact between the excited holes and AA, resulting in a high sensitivity of the sensor.

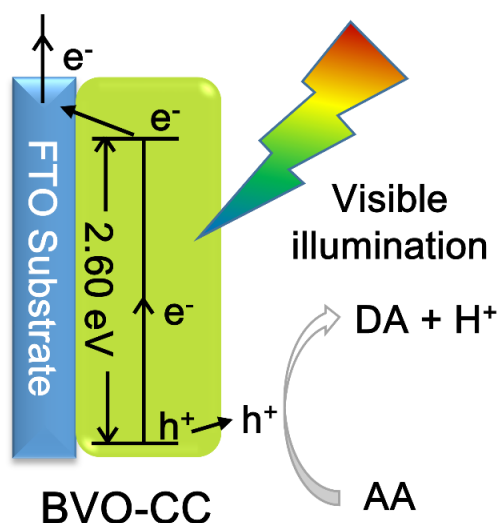


**Figure 22.** Schematic illustration of the working mechanism for the nanoworm  $\text{BiVO}_4$  PEC sensor (BVO-CC).

#### 4. CONCLUSION

A photoelectrochemical sensor based on the nanoworm  $\text{BiVO}_4$  electrode was successfully prepared by sol-gel drop-casting. In the thermal process, cyanuric chloride that was introduced into the precursor solution bound the precursors, accounting for the construction of the precursor networks and

then the finally obtained porous BiVO<sub>4</sub>. The nanoworm morphology that was attributed to the calcination of the precursor networks led to the enhancement of light absorption and charge transfer efficiency. The nanoworm BiVO<sub>4</sub> photoanode enhanced the photocurrent density and exhibited a high sensitivity towards ascorbic acid.

#### ACKNOWLEDGMENTS

This work was financially supported by the National Natural Science Foundation of China (21773074) and the Guangdong Natural Science Foundation (2014A030311039).

#### References

1. A.M. Pisoschi, A. Pop, A.I. Serban, and C. Fafaneata, *Electrochim. Acta*, 121 (2014) 443.
2. F. Yang, J. Wang, Y. Cao, L. Zhang, and X. Zhang, *Sensor. Actuat. B-Chem.*, 205 (2014) 20.
3. L.C. Jiang, and W.D. Zhang, *Biosens. Bioelectron.*, 25 (2010) 1402.
4. N.K. Bhajanthri, V.K. Arumugam, R. Chokkareddy, and G.G. Redhi, *J. Mol. Liq.*, 222 (2016) 370.
5. W.-D. Zhang, J. Chen, L.-C. Jiang, Y.-X. Yu, and J.-Q. Zhang, *Microchim. Acta*, 168 (2010) 259.
6. R. Saravanan, M.M. Khan, V.K. Gupta, E. Mosquera, F. Gracia, V. Narayanan, and A. Stephen, *RSC Adv.*, 5 (2015) 34645.
7. W. Ma, D. Han, M. Zhou, H. Sun, L. Wang, X. Dong, and L. Niu, *Chem. Sci.*, 5 (2014) 3946.
8. B. Sun, K. Zhang, L. Chen, L. Guo, and S. Ai, *Biosens. Bioelectron.*, 44 (2013) 48.
9. K.O. Akihiko Kudo, and Hideki Kato, *Journal of the American Chemical Society*, 121 (1999) 11459.
10. H.K. Saimi Tokunaga, and Akihiko Kudo, *Chem. Mater.*, 13 (2001) 4624.
11. J. Yu, and A. Kudo, *Adv. Funct. Mater.*, 16 (2006) 2163.
12. Q.-Y. Zeng, J.-H. Li, L.-S. Li, J. Bai, L.-G. Xia, and B.-X. Zhou, *Appl. Catal. B-Environ.*, 217 (2017) 21.
13. A. Iwase, S. Yoshino, T. Takayama, Y.H. Ng, R. Amal, and A. Kudo, *Journal of the American Chemical Society*, 138 (2016) 10260.
14. Y. Sun, C. Wu, R. Long, Y. Cui, S. Zhang, and Y. Xie, *Chem. Commun.*, (2009) 4542.
15. Y. Zhao, Y. Xie, X. Zhu, S. Yan, and S. Wang, *Chem. Eur. J.*, 14 (2008) 1601.
16. L. Wang, D. Han, S. Ni, W. Ma, W. Wang, and L. Niu, *Chem. Sci.*, 6 (2015) 6632.
17. M. Liu, Y.X. Yu, and W.D. Zhang, *Electroanal.*, 29 (2017) 305.
18. E. Singh, M. Meyyappan, and H.S. Nalwa, *ACS. Appl. Mater. Inter.*, 9 (2017).
19. T.W. Kim, and K.S. Choi, *Science*, 343 (2014) 990.
20. Y. Kuang, Q. Jia, H. Nishiyama, T. Yamada, A. Kudo, and K. Domen, *Adv. Energy Mater.*, 6 (2016) 1501645.
21. C. Feng, Z. Jiao, S. Li, Y. Zhang, and Y. Bi, *Nanoscale*, 7 (2015) 20374.
22. K.J. McDonald, and K.S. Choi, *Energ. Environ. Sci.*, 5 (2012) 8553.
23. S.J. Hong, S. Lee, J.S. Jang, and J.S. Lee, *Energ. Environ. Sci.*, 4 (2011) 1781.
24. X. Zhang, B. Zhang, K. Cao, J. Brillet, J. Chen, M. Wang, and Y. Shen, *J. Mater. Chem. A*, 3 (2015) 21630.
25. Y. Pihosh, I. Turkevych, K. Mawatari, J. Uemura, Y. Kazoe, S. Kosar, K. Makita, T. Sugaya, T. Matsui, D. Fujita, M. Tosa, M. Kondo, and T. Kitamori, *Sci. Rep.*, 5 (2015) 11141.
26. L. Yan, W. Zhao, and Z. Liu, *Dalton T.*, 45 (2016) 11346.
27. G. Blotny, *Tetrahedron*, 62 (2006) 9507.
28. Z.E. Koç, *J. Heterocyclic. Chem.*, 48 (2011) 769.
29. Y.O. Tadashi Wantanabe, Hirohiko Tsuzuki, Shoichiro Yoshida, and Yoshimasa Nihei, *Chem. Lett.* (1988) 1183.

30. T.E. Chien, K.L. Li, P.Y. Lin, and J.L. Lin, *Langmuir*, 32 (2016) 5306.
31. S. Lee, I.S. Cho, J.H. Lee, D.H. Kim, D.W. Kim, J.Y. Kim, H. Shin, J.-K. Lee, H.S. Jung, N.-G. Park, K. Kim, M.J. Ko, and K.S. Hong, *Chem. Mater.*, 22 (2010) 1958.
32. F.Y. Su, C.Q. Xu, Y.X. Yu, and W.D. Zhang, *Chem. Cat. Chem.*, 8 (2016) 3527.
33. P.C. Song-Can Wang, Jung-Ho Yun, Yu-Xiang Hu, and Lian-Zhou Wang, *Angew. Chem.*, 129 (2017) 8620.
34. U.M. García-Pérez, S. Sepúlveda-Guzmán, and A. Martínez-de la Cruz, *Solid State Sci.*, 14 (2012) 293.
35. W. Liu, Y. Yu, L. Cao, G. Su, X. Liu, L. Zhang, and Y. Wang, *J. Hazard. Mater.*, 181 (2010) 1102.
36. K. Li, X. Xie, and W.D. Zhang, *Carbon*, 110 (2016) 356.
37. X.Z. Tang, W. Li, Z.Z. Yu, M.A. Rafiee, J. Rafiee, F. Yavari, and N. Koratkar, *Carbon*, 49 (2011) 1258.
38. H. Raissi, A. Nowroozi, R. Mohammadi, and M. Hakimi, *Spectrochim. Acta A*, 65 (2006) 605.
39. D.W. Su, S.X. Dou, and G.X. Wang, *J. Mater. Chem. A*, 2 (2014) 11185.
40. Y. Wang, S. Li, X. Xing, F. Huang, Y. Shen, A. Xie, X. Wang, and J. Zhang, *Chem. Eur. J.*, 17 (2011) 4802.
41. K. Li, F.Y. Su, and W.D. Zhang, *Appl. Surf. Sci.*, 375 (2016) 110.
42. Y. Liu, D.P. Wang, Y.X. Yu, and W.D. Zhang, *Int. J. Hydrogen Energy* 37 (2012) 9566.
43. G.P. Keeley, A. O'Neill, N. McEvoy, Nikos Peltekis, J.N. Coleman, and G.S. Duesberg, *J. Mater. Chem.*, 20 (2010) 7864.
44. Z.H. Sheng, X.Q. Zheng, J.Y. Xu, W.J. Bao, F.B. Wang, and X.H. Xia, *Biosens. Bioelectron.*, 34 (2012).
45. J. Lavanya, and N. Gomathi, *Talanta*, 144 (2015).
46. D. Zhao, G. Yu, K. Tian, and C. Xu, *Biosens. Bioelectron.*, 82 (2016).

© 2019 The Authors. Published by ESG ([www.electrochemsci.org](http://www.electrochemsci.org)). This article is an open access article distributed under the terms and conditions of the Creative Commons Attribution license (<http://creativecommons.org/licenses/by/4.0/>).